Sunflower Proteins at Air–Water and Oil–Water Interfaces

Alexandre Poirier, Antonio Stocco, Romain Kapel, Martin In, Laurence Ramos, Amélie Banc

Sunflower proteins at air-water and oil-water interfaces

A. Poirier[1], A. Stocco[1,2], R. Kapel[3], M. In[1], L. Ramos[1], A. Banc[1*]

[1] *Laboratoire Charles Coulomb (L2C), Univ. Montpellier, CNRS, Montpellier, France.*

[2] *Institut Charles Sadron (ICS), CNRS-UPR22, 23 rue du Loess BP 84047, 67034 Strasbourg Cedex 2, France*

[3] *Laboratoire Réactions et Génie des Procédés (LRGP), Site Plateforme Sciences du Vivant et de la Santé, 54500 Vandoeuvre-les-Nancy, France*

*Corresponding author email address : amelie.banc@umontpellier.fr

Abstract

The adsorption of a sunflower protein extract at two air-water and oil-water interfaces is investigated using tensiometry, dilational visco-elasticity and ellipsometry. For both interfaces, a three step mechanism was evidenced thanks to master curve representations of the data taken at different ageing times and protein concentrations. At short time, a diffusion limited adsorption of proteins at interfaces is demonstrated. Firstly, a 2-dimensional protein film is formed with a partition of the polypeptide chains in the two phases that depends strongly on the nature of the hydrophobic phase: most of the film is in the aqueous phase at the air-water interface, while it is mostly in the organic phase at the oil-water interface. Then a 3-dimensional saturated monolayer of proteins is formed. At short time adsorption mechanisms are analogous to those found with typical globular proteins while strong divergences are observed at longer adsorption times. Following the saturation step, a thick layer expands in the aqueous phase and appears associated to the release of large objects in the bulk. The kinetic evolution of this second layer is compatible with a diffusion limited adsorption of the minor population of polymeric complexes with hydrodynamic radius $R_H \sim 80$ nm, evidenced in equilibrium with hexameric globulins ($R_H \sim 6$ nm) in solution. These complexes could result from the presence of residual polyphenols in the extract, and raise the question of the role of these compounds in the interfacial properties of plant protein extracts.

Keywords: Sunflower globulin, plant protein, polyphenolic compounds, air-water, oil-water interface, tensiometry, dilational rheology, ellipsometry, master curve.

1. Introduction

Proteins are of great interest due to their amphiphilic nature, which allows them to reduce the interfacial tension of air-water and oil-water interfaces. They are extensively used to stabilize fluid-liquid interfaces in foams and emulsions. Considering the current environmental and demographical issues, plant proteins represent an alternative source of proteins for human food consumption [1], and for the production of functional ingredients for food, personal care and pharmaceutical industries [2]. However, the use of plant proteins remains challenging. Many plant proteins are difficult to extract and purify at the industrial scale due to their insolubilities in aqueous solutions and/or strong interactions with different components. In particular, extraction processes can induce a partial denaturation of proteins, and leave different residual impurities difficult to remove, like phenolic compounds[3]. For these reasons, bulk and interfacial properties of plant proteins have been much less exploited in industrial products and are also, from a more fundamental perspective, less studied than their animal counterpart [4-5].

The large size of proteins, their different amphipathicity, charge distribution and flexibility make their adsorption behavior specific to each protein. Nevertheless, using highly purified animal proteins, two main families of proteins were identified relative to their interfacial behavior: “hard proteins” which generally correspond to globular proteins, and “soft proteins” which correspond to proteins including more disordered domains along their sequence. “Hard proteins” are found to behave more like colloidal particles, and include bovin serum albumim, lysozyme, β-lactoglobulin, ovalbumin. By contrast, “soft proteins”, which behave more like polymers, include β-casein [6-10]. The “hard” or “soft” behaviors of the proteins come from their structural flexibility. Hard proteins display a high internal stability which limits structural changes during adsorption contrary to soft proteins that show a low internal stability and can easily undergo structural changes. However, this

binary classification appears restrictive and some authors [4] proposed to consider the thermodynamic stability using the instability index (II) [11] computed to predict protein's metabolic stability in vivo in correlation with the amino-acid sequence.

In this framework, a detailed understanding of the formation and structural rearrangement of plant proteins film appears essential to identify potential specificities of plant sourced proteins, and eventually predict, control and optimize the formulation of foams and emulsions, which is crucial for industrial applications.

Sunflower represents an interesting source of proteins as this crop is the fourth worldwide production for edible oil trade (http://www.fediol.eu), and the meal, the major byproduct of sunflower oil industry, contains about 30% (w/w) proteins [12]. The sunflower meal is presently mainly used for animal feed but the low content of antinutritional factors and the absence of toxic substances in sunflower meal would make it useful for human consumption[13]. The two main groups of proteins present in the sunflower meal can be classified according to their sedimentation coefficient: sunflower globulins 11S, called helianthinin [14], and sunflower albumins 2S [15]. According to the Osborne classification, globulins are soluble in salted water while albumins are soluble in water. Sunflower globulin is an anti-trigonal prism hexamer with a radius of gyration close to 5 nm [16] and is known to be the main sunflower storage protein. This hexamer has an isoelectric point of 5.5 and a molecular weight close to 300kDa. It can be dissociated in trimers (7S form) or monomers (3S form) depending on the composition of the solvent and the process used to prepare the protein dispersion [17]. Each monomer consists in two polypeptides chains linked by a single disulfide bond [18]. On the other hand, sunflower albumin has an average isoelectric point of 8.8 and a molecular weight of 10 – 18 kDa. It is formed by two polypeptides chains linked by two disulfide bonds [13]. Both sunflower globulin and albumin are classified as globular proteins.

It has been previously shown that sunflower meals and protein isolates can stabilize foams and emulsions with performances comparable to soy, one of the most used and investigated plant proteins (see ref [13] and references cited therein). However, contradicting results concerning the comparative performances of the different sunflower protein preparations strongly suggest that extraction processes significantly impact the overall performance due to uncontrolled contents of denatured proteins and phenolic compounds [19-20].

In this paper we investigate with a multiscale approach the adsorption behavior at air-water and oil-water interfaces of a sunflower isolate rich in globulin. Detailed analyses of the time evolution

of the surface pressure, the viscoelastic moduli, and the ellipsometric signal, lead to a consistent interpretation of the successive steps in the formation of an interfacial protein film and of the associated structures. We show that sunflower proteins form a saturated monolayer at both interfaces following a diffusive adsorption mechanism but with a higher degree of unfolding at the oil-water interface than at the air-water interface. However, more specifically to this plant extract, a thick interfacial layer is shown to form in the aqueous phase at long adsorption times and to release large objects in the bulk. This long time mechanism appears associated to the presence of polymeric assemblies in the bulk that could be formed because of the interaction between proteins and residual phenolic compounds.

2. Experimental section

2.1. Material

Sunflower proteins extraction and characterization

The production of the sunflower protein isolate is obtained from an industrial sunflower meal defatted by hexane. A solid/liquid extraction step followed by a purification step with an ultrafiltration process is used to isolate proteins. The solid/liquid extraction is performed by mixing sunflower meal with 1 M NaCl respecting a 1:9 solid/liquid ratio. The pH is adjusted to 7.0 (±0.5) by adding 1 M NaOH. The mixture is stirred at 400 rpm during 30 min and then centrifuged (15 000×g, 30 min, 20 °C). The resulting supernatant, referred to as the liquid extract, is additionally clarified using a Whatman filter paper. An ultrafiltration step is then carried out using an Akta Flux® 6 system from GE Healthcare (Chicago, IL, USA) coupled with 3 kDa cut-off, 0.1 m^2 Pellicon 2 Mini Ultrafiltration Module PLBC C from Millipore (Burlington, MA, USA). First, the liquid extract is washed with 7 diafiltration volumes of an aqueous solution with 0.5 M NaCl. Then, the pH of the retentate is adjusted to 10 using 1 M NaOH and the retentate is washed with 3 diafiltration volumes of ultrapure water. The final retentate is collected and freeze-dried. The dry matter of the isolate corresponds to 90% w/w and the protein content is 85% w/w according to the Kjeldahl method. The globulin/albumin ratio in the sunflower protein isolate is 4 according to the SE-HPLC method of Defaix et al[21] (see supplementary information Figure SI1a). Polyphenols compounds are quantified according to the SE-HPLC method of Albe Slabi et al[22]: the extract

contains 1.7% w/w free chlorogenic acids and 1.53% w/w polyphenols bonded to proteins (18.3 mg per one gram of proteins). Other impurities include salts and residual cellulosic fibers.

The solubility of the extract depends on the pH of the solvent (see supplementary information Figure SI1b). In agreement with previous studies [17, 23], we find that the globulin-rich extract displays a minimum of solubility around pH 5, which corresponds to the isoelectric point of sunflower globulins estimated between 5 and 5.9. By contrast, the extract is soluble up to 90% in acid (pH < 2) and basic conditions (pH > 8). As a consequence, to get clear solutions of the isolate, we choose to fix the pH of all samples at 10. At this pH the net charge of globulins is +12 according to the subunit sequence P19084 and globulins are in their hexameric form according to the thermogram of a protein suspension measured by micro differential scanning calorimetry (see supplementary information Fig. SI1c).

Sample preparation

We use a 10^{-4} M NaOH aqueous solution (pH 10) as a solvent to solubilize the sunflower isolate. We prepare suspensions of protein isolate with concentration C in the range (0.001-100) g/L. Concentrated samples (C > 10 g/L) are prepared by dispersing, with a few seconds gentle manual agitation, the appropriate amount of isolate in the aqueous solvent, and filtering the suspension with a 0.22 µm cellulose mixed ester membrane. Low concentration solutions (C < 10 g/L) are prepared by dilution of a stock solution at C = 10 g/L. After a few seconds of gentle manual agitation, all solutions are transparent and yellow to dark colored. For measurements at the oil/water interface, we use anhydrous hexadecane (purity 99 %). To get a stable surface tension (with variation less than 2 mN/m over 1 hour for the bare hexadecane-water interface), we previously saturate and clean the hexadecane by vigorously mixing during 1 minute 1 volume of hexadecane with 3 volumes of milliQ water in the presence of 1 volume of air, and then let the mixture decant for 12 h before removing the aqueous phase using a separating funnel.

Dielectric constant and refractive index of the samples

The refractive index of the protein solutions in the visible range, n_{bulk}, is measured with an Abbe refractometer, for protein concentrations C from 0 to 100 g/L. Concentrations are converted in volume fraction of dry protein, ϕ_B, assuming a protein relative density ρ_P = 1.35 [24-25]. For ϕ_B in

the range (0-0.074), the data can be very well accounted for by a linear variation of n^2_{bulk} with ϕ_B, as predicted theoretically (see Figure SI1d in supplementary information). In the Wiener effective medium approximation [26], the dielectric constant $\varepsilon = n^2$ (with n the refractive index) is indeed expected to change linearly with ϕ_B. Hence the refractive index of the protein solutions, n_{bulk}, reads

$$n^2_{\text{bulk}}(\phi_B) = n^2_{\text{solv}}\,(1-\phi_B) + n^2_{\text{prot}}\,\phi_B \qquad \text{(Eq. 1)}$$

with $n_{\text{solv}} = 1.333$ the index of refraction of the solvent, and n_{prot} the index of refraction of the proteins. Equation 1 can be rewritten as

$$n^2_{\text{bulk}}(\phi_B) = n^2_{\text{solv}} + \phi_B\left(n^2_{\text{prot}} - n^2_{\text{solv}}\right) = n^2_{\text{solv}} + \frac{\Delta(n^2)}{\Delta\phi}\phi_B \qquad \text{(Eq. 2)}$$

The best fit of the experimental data ($n^2_{bulk}=f(\Phi_B)$, see SI1d in supplementary information) to Eq. 2 yields the slope $\frac{\Delta(n^2)}{\Delta\phi} = 0.48 \pm 0.02$, giving an index of refraction of the proteins, $n_{\text{prot}} = \sqrt{n^2_{\text{solv}} + \frac{\Delta n^2}{\Delta\phi}} = 1.50 \pm 0.01$.

2.2. Methods

Dynamic light scattering

Dynamic light scattering (DLS) is performed using a laser beam with an incident wavelength $\lambda = 532$ nm, a power of 50 mW and a pinhole of 1 mm. Measurements are carried out for 21 scattering angles, θ, ranging between 30 and 130° using an Amtec goniometer, yielding wavevectors $q = \frac{4\pi n}{\lambda}\sin\frac{\theta}{2}$ ranging between 5.10^6 and 3.10^7 m^{-1}. The intensity auto-correlation functions, $g_2(\tau)$-1, are calculated using a Brookhaven BT9000 correlator for delay times, τ, in the range (10^{-7} - 10^{-2}) s. Correlation functions are analyzed using a double exponential function: $g_2(\tau) - 1 = (A_s e^{-\Gamma_s \tau} + A_f e^{-\Gamma_f \tau})^2$, where Γ_s and Γ_f are the decay rates, and A_s and A_f, the amplitudes, corresponding respectively to the slow and the fast populations of a bimodal distribution of scattering objects.

Pendant drop tensiometry

A drop profile analysis tensiometer (PAT-1, SINTERFACE Technologies, Germany) is used for surface tension and surface dilational rheology measurements. An aqueous pendant drop (typical volume comprised between 46 mm^3 and 60 mm^3, respectively 17 mm^3 and 30 mm^3 for oil-water,

respectively air-water, interface) is formed at the capillary tip (of diameter 2 mm) inside a measuring glass cell (32x35x35 mm^3) filled with air or hexadecane. The images of the drop are recorded and the interfacial tension is computed from the shape of the drop [27]. The surface pressure is defined as $\Pi = \gamma_{solv} - \gamma$, where γ_{solv} is the interfacial tension of the solvent in the absence of protein (γ_{air} = 73 mN/m and γ_{oil} = 47 mN/m) and γ is the interfacial tension of the protein solution against air or hexadecane. The analysis of the images of the drop for quantifying its turbidity is performed using ImageJ software.

Dilational rheology measurements

We use the drop profile tensiometer to study the dilational rheology of proteins at interfaces. To do so, an aqueous drop is perturbed by small harmonic oscillations of the interfacial area A of pulsation ω leading to harmonic oscillations of the surface tension γ. From the Fourier transform F of the response relative to the perturbation the complex visco-elastic modulus E is calculated [28]:

$$E(i\omega) = \frac{F[\Delta\gamma]}{F[\Delta \ln(A)]} \qquad \text{(Eq. 3)}$$

where $F[\Delta\gamma]$ is the Fourier transform of $\Delta\gamma = \gamma(t) - \langle\gamma(t)\rangle_{t_m}$ with $\langle\gamma(t)\rangle_{t_m}$ the temporal average of surface tension over a duration t_m, and $\Delta \ln(A) = \frac{A(t)-\langle A(t)\rangle_{t_m}}{\langle A(t)\rangle_{t_m}}$ with $\langle A(t)\rangle_{t_m}$ the temporal average of the interfacial area over t_m.

The real part of $E(i\omega)$, E', is the storage modulus that characterizes the dilational interfacial elasticity, and the imaginary part, E'', is the loss modulus and is related to the dilational interfacial viscosity. We impose relative deformations $\frac{\Delta A}{A}$ of 5 %, at a frequency of 0.1 Hz for all samples. These parameters are chosen to optimize the quality of raw data while remaining in the linear regime of the response.

Ellipsometry

Air-water and oil-water planar interfaces are prepared to investigate the structure of the interfacial protein films by ellipsometry. A glass Petri dish of diameter 17 cm is filled either directly with protein solution for the air-water interface, or previously filled with hexadecane and then filled with the aqueous solution for the oil-water interface. Then, interfaces are cleaned by a careful aspiration with a micropipette connected to a pump just before the beginning of optical data

acquisition. The origin of time for protein adsorption, t_0, is therefore associated to the end of the cleaning step.

An ellipsometer (Optrel, Germany) using a green laser light (wavelength λ = 533 nm) with the power set at 20 mW, respectively 100 mW, for the air-water, respectively oil-water interface, is used. To access the liquid-liquid interface without any distortion of the optical path, the ellipsometer is equipped with optical wave guides for measurements at the oil-water interface. The angles Ψ and Δ are measured by nulling ellipsometry. Ψ and Δ are related to the ratio of reflection field coefficients $\frac{r_p}{r_s}$ by:

$$\frac{r_p}{r_s} = \tan\Psi \exp i\Delta \qquad \text{(Eq. 4)}$$

Here r_p is the component of field reflection coefficient parallel to the reflection plane, and r_s is the component perpendicular to reflection plane.

The Brewster angle θ_B is the incident angle associated to the minimum value of $\tan\Psi$. The Brewster angle of the interfaces is determined measuring Ψ and Δ as a function of the laser beam incident angle φ. We quantify the deviation of the Brewster angle $\Delta\theta$ from that of the bare interface when proteins are adsorbed. If this deviation is lower than 0.1°, a numerical value related to the accuracy of the measurement, data are analyzed in the framework of the perturbation theory. Ellipsometric data showing a clear shift of the minimum value of $\tan\Psi$ (>0.1°) cannot be described by the perturbation theory, and are instead analyzed using the classical stratified layer model.

When experimental conditions lead to a Brewster angle that is nearly not deviated from that of the bare interface, the quantities Ψ and Δ are measured as a function of adsorption time at a unique incident angle, φ_{Air} = 55°, respectively φ_{Oil} = 45° for air-water, respectively oil-water, interface. Perturbation theory describes $\frac{r_p}{r_s}$ as the deviation from the reflection coefficient $\frac{r_{p,0}}{r_{s,0}}$ expected for a sharp step-like profile[29]:

$$\frac{r_p}{r_s} = \frac{r_{p,0}}{r_{s,0}} + \frac{2iQ_{Air/Oil}}{r_{s,0}\left(Q_{Air/Oil}+Q_{bulk}\right)^2}\frac{K^2}{n_{Air/Oil}^2\, n_{bulk}^2} I_1 \qquad \text{(Eq. 5)}$$

Here $Q_{Air/Oil} = \frac{2\pi}{\lambda n_{Air/Oil}}\cos\varphi_{Air/Oil}$, $Q_{bulk} = \frac{2\pi}{\lambda n_{Bulk}}\cos\varphi_{Bulk}$ and $K = = \frac{2\pi n_{Air/Oil}}{\lambda}\sin\varphi_{Air/Oil}$, where n_i are the refractive indexes and φ_i are the angles of the beam relative to the normal of the interface in the propagating media i. Indices *bulk* and *Air/Oil* are associated to the bulk aqueous

media and the air or oil media depending on the type of interface considered. $\varphi_{Air/Oil}$ and $\varphi_{bulk,}$ are related by the Snell's law: $n_{Air/Oil} \sin \varphi_{Air/Oil} = n_{bulk} \sin \varphi_{bulk}$. Considering that the interfacial layer (protein film) is locally isotropic, the term I_1 is related to the interfacial optical profile as [29]:

$$I_1 = \int_{-\infty}^{+\infty} \frac{\left(n_L^2(z) - n_{Air/Oil}^2\right)(n_L^2(z) - n_{bulk}^2)}{n_L^2(z)} dz \qquad \text{(Eq. 6)}$$

Here z is the axis normal to the interface (with the convention $z > 0$ in the top fluid, air or oil) and $z = 0$ is the location of the Gibbs dividing surface, $n_L(z)$ is the refractive index of the interfacial layer as a function of the distance z from the interface. Hence, I_1 couples information on the refractive index $n_L(z)$ of the interfacial layer and on its thickness. Using some approximations (detailed in the Experimental results section below), the term I_1 can be related in some cases to the surface excess concentration Γ of proteins at the interface defined as:

$$\Gamma = \int_{-\infty}^{0} (c(z) - C)\, dz + \int_{0}^{+\infty} c(z)\, dz \qquad \text{(Eq. 7)}$$

Here $c(z)$ is the solute concentration as a function of the distance z from the interface and C the solute concentration in the bulk solution [$C = c(z \ll 0)$].

When the Brewster angle of the interface with adsorbed proteins significantly deviates from the bare interface, the multi-angle ellipsometric measurements (Ψ and Δ as a function of $\varphi_{Air/Oil}$) are modelled by the commonly used stratified layer model [30] considering a single homogeneous and isotropic layer. In the Fresnel equations for r_P and r_s reflection coefficients, the interfacial layer is described by a thickness H and an interfacial refractive index n_L.

3. Results and discussion

3.1. Experimental results

Diffusion of proteins in the bulk

Bulk protein solutions are investigated by DLS. Correlation functions measured at different angles are displayed in Figure 1a for a solution of protein isolate with concentration C = 5 g/L. The

functions cannot be correctly fitted with a cumulant analysis which implies a monomodal distribution of sizes. Instead, experimental data are well accounted for with a double exponential model that considers a bimodal distribution (see methods). The fast, Γ_f, and slow, Γ_s, decay rates, are plotted as a function of the wavevector q in log-log scale in Figure 1b. The decay rates are proportional to q^2, as expected for diffusive processes. The proportionality factors are the translation diffusion coefficients D, which are related to the hydrodynamic radii, R_H, of spherical objects via the Stokes-Einstein relation, $D = \frac{k_B T}{6\pi\eta_0 R_H}$, where $k_B T$ is the thermal energy and η_0 is the solvent viscosity (η_0 = 1 mPa s). Here, we measure D_f = (35±5) μm²/s and D_s = (2.8±0.4) μm²/s, leading to $R_{H,f}$ = (6 ± 1) nm and $R_{H,s}$ = (77 ± 10) nm. The small size is consistent with the radius of gyration of sunflower globulin hexamers (R_g = 5 nm) [16] while the second size can be attributed to complexes. Interestingly, while Γ_f is proportional to q² in the whole q range, Γ_s displays two regimes: at small q, a q^2 dependence is measured, whereas the increase is faster than q^2 at large q. This feature is the sign that, in addition to translation diffusion, other mechanisms occur, leading to a faster relaxation of the correlation functions. The departure from the q^2 dependence occurs roughly when qR_H becomes larger than 1, hence when one probes the dynamic of the scattering objects at length scale smaller than their size suggesting an internal dynamic for the scattering objects. This implies that the large objects are not compact bodies. Notably, our data present strong analogies with data obtained for linear or branched synthetic polymer coils [31], but also for more complex natural polymers [32-33]. At high q, the relaxation rate is found to vary as a power law with the wave vector close to q^3, as theoretically expected for polymers [34], and is the signature of objects with a low density.

The weight fraction of the two populations is encoded in the amplitude of the fast and slow modes. For spherical colloidal particles, the amplitude A_i (where the subscript i stands for either s, the slow population or f, the fast population) is proportional to $N_i V_i^2 P_i(q) \propto w_i R_i^3 P_i(q)$, with N_i the number of objects i in the irradiated volume, V_i the volume, R_i the radius, w_i the weight fraction and $P_i(q)$ the form factor of the scattering objects i [35]. By contrast, for linear polymer chains the amplitude is proportional to $A_i \propto c_i M_i P_i(q)$ with c_i the mass concentration and M_i the weight average molecular weight of polymer chains i. Depending on the solvent quality for the polymer, according to the Flory prediction [36], M_i is related to the radius of gyration R_{gi}: $A_i \propto c_i R_{gi}^{\nu} P_i(q)$ with $\nu = 2$ for polymer chains in a theta solvent and $\nu = 5/3$ in a good solvent [35]. At very low q ($qR_g < \sqrt{3}$ for polymers and

$qR < 1.78$ for spherical particles), $Pi(q) \rightarrow 1$ and an expression of the weight fraction of the slow population can be estimated from the relative amplitudes of the correlation function assuming a same nature for the slow and the fast populations [35]:

$$w_S = \frac{\frac{A_S/(A_S+A_f)}{R_S^\beta}}{\frac{A_S/(A_S+A_f)}{R_S^\beta}+\frac{A_f/(A_S+A_f)}{R_f^\beta}} \qquad \text{(Eq. 8)}$$

When scattering objects are polymers, R_i is the radius of gyration of population i, and $\beta = 2$ for theta solvent and $\beta = 5/3$ for good solvent. Instead, if scattering objects are particles, R_i is the radius of population i and $\beta = 3$. Using Eq. 8 with the relative amplitude extrapolated to $q = 0$ as shown in the inset of Figure 1b and using hydrodynamic radii instead of R_i, we can derive a rough estimation of the weight fraction of the slow population. We find $w_s = 0.2$ % considering spherical particles, $w_s = 3$ % considering polymers in theta solvent and $w_s = 6$ % considering polymers in good solvent. In all cases, we evaluate a small fraction of large objects; it is however difficult to provide a reliable precise value. Indeed, on one hand, globulins are globular proteins that can be considered as colloidal particles, but on the other hand, the slow population displays an internal dynamics similar to polymers. In conclusion, the analysis of the protein solution shows that the hexameric form of globulins is the dominant population in bulk but polymeric assemblies of typical size 80 nm are also present.

Surface pressure

We show in Figures 2a,b the time evolutions over 1 hour of the air-water and oil-water surface pressures, as measured for several protein concentrations in the aqueous phase, using the pendant drop tensiometry. For the lowest protein concentrations ($C < 1$ g/L for air-water interface and $C < 0.2$ g/L for oil-water interface), an induction period, corresponding to a null surface pressure, is measured. The duration of this period decreases with the bulk protein concentration. The induction period is then followed by a sharp increase of the surface pressure Π until reaching a pseudo plateau at Π_p. The pseudo-plateau regions are shown as horizontal colored bands in Figures 2a,b. We measure $\Pi_p = (15\pm2)$ mN/m for the air-water interface, and $\Pi_p = (22\pm2)$ mN/m for the oil-water interface. For the highest protein concentrations, the pseudo-plateau is finally followed by a second increase of the surface pressure. Interestingly, all the data gathered with a given interface overlap on a single master curve once plotted as a function of a normalized time αt, where t is the actual

time defined as the time elapsed since the drop formation, and α is a scaling factor (Fig. 2c). Master curves of similar shape are observed for the two interfaces. The two master curves evidences three regimes characterized by distinctive features: regime I is the induction period followed by a sharp increase of the surface pressure Π, regime II is the pseudo-plateau of Π and regime III corresponds to the second increase of Π. At the oil-water interface the first regime is shorter and the surface pressures reached are higher than at the air-water interface. This suggests that proteins are more surface active at an oil-water interface than at an air-water interface. The scaling factors used to build the two master curves are displayed in Figure 2d and are compared to the evolution expected for a kinetic dominated by a diffusive process [37]: $\alpha = (C/C_{ref})^2$ (we have arbitrarily chosen $C_{ref}=0.1$ g/L) For $C < 0.5$ g/L, the time-concentration superposition is found to hold and scaling factors are in a very good accordance with the diffusive model. By contrast, we find that for data corresponding to $C > 0.5$ g/L, which cover the third regime, the data overlap is not as good (especially for the oil-water interface). The departure from a satisfying overlap strongly suggests that, in this regime, the protein film evolution is not only governed by the protein concentration in the bulk, but also depends on the age and/or history of the interfacial film.

Dilational viscoelasticity of the protein interfacial layer

The dilational viscoelasticity of the protein films at different times after the drop formation, and for various protein concentrations in the aqueous phase, is measured. The elastic moduli (E'), loss moduli (E'') and the ratio E''/E' are plotted as a function of the surface pressure in Figure 3. For both air/water and oil/water interfaces, until the pseudo plateau for the surface pressure at Π_p (as evidenced by vertical bands in the graphs), all data fall onto a single master curve. In regime I, as defined with the time evolution of the surface pressure (Fig. 2), the protein films are mainly elastic since E''/E' is very small (<0.1). In this regime, at low Π, the elastic moduli display a linear evolution with surface pressure: $E'=p\Pi$. The values of the proportionality constant p can be interpreted in term of Flory exponents derived at interfaces for polymers in the semi-dilute regime[38-39]. The theoretically expected values for polymers forming 2-dimensional (2D), resp. 3-dimensional (3D) films, are p=8, respectively p=3 in theta solvent, and p=3, respectively p=2.25 in good solvent. At low Π, we find p=9 ±2 for an air-water interface and p=3.4±0.6 for an oil-water interface. The experimental values measured at low surface pressure suggest therefore that the

protein films can be considered as 2D-structures made of polymers in theta solvent at the air-water interface and in good solvent conditions at the oil-water interface. These findings indicate that sunflower proteins are initially adsorbed flat on the interface with a higher compacity for an air-water interface than for an oil-water interface. Still in regime I, the linear increase of E' is followed by a nearly stationary evolution of E' with Π, suggesting a weak evolution of the protein film structure. In regime II, a second linear evolution of E' with Π is measured with a smaller proportionality constant than the one measured at small surface pressure: p=3.0±0.2, respectively p=2.0±0.1, for air-water, respectively oil-water, interface. According to Flory exponents at interfaces, the decrease of p can be interpreted in terms of the development of the protein film in 3D. In addition, for both interfaces the pseudo-plateau regime (regime II) is characterized by a maximum of the loss moduli, indicative of relaxation processes. Interestingly, no master curve could be obtained above Π_p for the elastic moduli. Instead, for both interfaces, we measure that, for a given protein concentration C, E' increases with Π, but data are shifted towards lower values as C increases. As for tensiometry measurements, the departure from data overlap indicates that in regime III the protein film is age and/or history-dependent and not only concentration-dependent and softer structures are formed with protein solutions of higher concentrations. In addition, in this regime the loss moduli are measured to decrease with the surface pressure, indicating more reduced dissipative processes.

Optical properties of the interfacial films

To get an additional insight on the protein films, we perform ellipsometry measurements on planar interfaces during the protein adsorption. In order to determine the most relevant model to interpret measurements, we first measure the deviation of the Brewster angle for one hour duration of protein adsorption. For bulk protein concentration $C \leq 10$ g/L, the Brewster angle deviation is lower than or equal to 0.1° considering errors bars (see Figure SI2 in supplementary information). Hence, the perturbation theory framework can be safely used for quantitative analyses of our experimental data. At both air-water and oil-water interfaces, for C in the range (0.005-10 g/L), we measure the deviation coefficient I_1 as a function of the adsorption time (Fig. 4). At air-water interface, I_1 is positive and increases with time and concentration. By contrast, for the oil-water interfaces, we find that I_1 is close to zero ($I_1 < 0.1$ nm whereas it reaches 1 nm at air-water interface) and becomes negative for C= 10 g/L. Interestingly, plotting I_1 as a function of the normalized time αt, using the

numerical values of α determined with tensiometry measurements (Fig. 2d), a continuous evolution of I_1 is evidenced at short rescaled times for both interfaces (Fig. 4c,d). The monotonous increase of I_1, interrupted by a pseudo-plateau at the air-water interface, is reminiscent of the surface pressure evolution. By contrast, at the oil-water interface, the increase of I_1 is much weaker and after a pseudo plateau, I_1 becomes negative. Interestingly, for both interfaces, the pseudo plateaus occur between $10^2 < \alpha t < 10^4$ s as in the surface pressure measurements.

Air-water interface

We start discussing the results obtained for air-water interfaces. Considering that proteins are mostly immersed in the aqueous phase, $n_{Air} << n_{bulk} < n_L$, small perturbation in the dielectric constant is induced by protein adsorption. Hence, following Eq. 6, at the air-water interface I_1 can be written as[40]:

$$I_1^{\text{Air-water}} \cong \Gamma_{n^2} \frac{n_{bulk}^2 - n_{Air}^2}{n_{bulk}^2} \quad \text{(Eq. 9)}$$

with $\Gamma_{n^2} = \int_{-\infty}^{\infty} (n_L^2(z) - n_{bulk}^2)\, dz$, the dielectric constant surface excess, which is directly related to the surface excess concentration Γ (Eq. 7) [41-42].

$$\Gamma \cong \frac{\Gamma_{n^2}}{\Delta n^2 / \Delta C} \cong \frac{I_1^{\text{Air-water}} \frac{n_{bulk}^2}{n_{bulk}^2 - n_{Air}^2}}{\Delta n^2 / \Delta C} \quad \text{(Eq. 10)}$$

The surface excess concentration at the air-water interface, as computed using Eq. 10, is plotted as a function of the normalized time in Figure 5. The curve displays a power law increase of Γ with αt at short normalized time ($\alpha t < 10^2$ s), before reaching a plateau at $\Gamma \sim 3$ mg/m^2. A second power law increase is measured at large normalized time ($\alpha t > 10^4$ s). The two power law exponents are close to ½, the exponent expected for diffusion-controlled adsorption processes. The intermediate plateau value on the other hand is indicative of a saturation step. Interestingly data are nicely fitted using an analytical model of diffusion-controlled adsorption kinetics with saturation [43] and comprising two independent diffusive populations:

$$\Gamma(t) = \Gamma_{mf}\left[1 - \exp\left(-\frac{2C(1-w_s)}{\Gamma_{mf}}\sqrt{\frac{D_f t}{\pi}}\right)\right] + \Gamma_{ms}\left[1 - \exp\left(-\frac{2Cw_s}{\Gamma_{ms}}\sqrt{\frac{D_s t}{\pi}}\right)\right] \quad \text{(Eq. 11)}$$

With D_i the bulk diffusion coefficients and Γ_{mi} the maximum surface excess concentrations with $i=f,s$, for fast and slow components. Equation 11 takes into account for each diffusing population the decreasing difference of chemical potential between bulk and interface along the adsorption process [44]. Hence at time long enough, with respect to the characteristic time for the diffusion of each population, a steady state is reached, corresponding to a saturation mechanism. The theoretical curve displayed in Figure 5 is the best fit of the experimental data points using Eq. 11, as obtained by setting the bulk diffusion coefficients measured by dynamic light scattering (D_f= (3.5±0.5) 10^{-11} m²/s, D_s = (2.8±0.4) µm²/s)), C = 0.1 g/L (the reference concentration of the rescaled data) and using Γ_{mf} , Γ_{ms} and w_s as fitting parameters. We find Γ_{mf} = 2.8 mg/m², Γ_{ms} = 4 mg/m² and w_s = 0.1. Hence the interface is firstly expected to be saturated mainly by the fast species (hexameric proteins) with a surface excess concentration at saturation typical for protein monolayers (2 < Γ < 3 mg/m²) [7, 45-46]. From Γ_{mf} we can define an area per protein at saturation and estimate the equivalent radius of proteins at saturation, R_{eq}, following simple geometric considerations:

$$R_{eq} = \sqrt{\frac{M_w}{\Gamma_{mf} N_A}} \qquad \text{(Eq. 12)}$$

with M_w the molar mass of hexamers (300 kg/mol) and N_A the Avogadro number. We find R_{eq} = 7.5 nm, a value close to the hydrodynamic radius measured in bulk (6 ± 1 nm). This suggests that proteins are weakly deformed in the interfacial film at saturation.

At longer times, large polymeric assemblies are expected to adsorb on the protein monolayer. Despite being of higher molar mass than the individual hexameric proteins, one measures a value at saturation (Γ_{ms} = 4 mg/m^2) only marginally larger than the one for the individual proteins. The saturation by the big objects is in agreement with the weak density of the assemblies, as inferred from the dynamic light scattering (DLS) measurements (Fig. 1). However, one must note that the numerical value for the surface excess concentration at saturation for the big objects has to be taken with caution as it is determined from values close to the limit of the perturbation theory. The mass fraction of the slow objects, w_s, on the other hand is fully consistent with the value obtained by DLS considering polymeric objects, thus reinforcing the validity of the model.

Oil-water interface

Because the refractive index of oil is higher than the one of air and is comparable to that of protein interfacial layer, the profile of the refractive index at an oil-water interface is very different from

the one at an air-water interface (Fig. 6). As a consequence, the approximations leading to Eq. 10 are not valid in that case. Thus, it is not possible to estimate the surface excess concentration from the optical signal I_1. However, significant qualitative information can be obtained exploiting Equation 6. First, we note that the time evolution of the ellipsometric signal cannot be interpreted considering that the protein film is only in the aqueous phase: in that case negative values of I_1 would be expected for low concentration protein films ($n_{bulk} < n_L < n_{oil}$) and positive values for high concentration films ($n_{bulk} < n_{oil} < n_L$), in sharp contrast with experimental findings. In addition, the hypothesis of a protein film totally in the oil phase is not more satisfying since I_1 would be expected positive whatever the protein concentration of the film ($n_{bulk} < n_{oil} < n_L$). Hence our data suggest that the proteins are partially immersed in the oil phase.

Partly immersed film model

For consistency of the analysis of the data acquired with the two interfaces, we systematically consider in the following that the protein film at interfaces is partly in the aqueous phase and partly in the second media (air or oil) (Fig. 6) Considering the refractive indexes of air (n_{air} = 1) and oil (hexadecane) (n_{oil} = 1.432), very different two-step refractive index profiles are expected, as represented in Figure 6 for an arbitrary volume fraction of protein fraction in film (ϕ_P = 39 %). The protein film is therefore decomposed into the sum of a layer of thickness $H\ \Phi_w$ in water, and a layer of thickness $H\ (1- f_w)$ in air or oil. Here H is the total interfacial protein film thickness, and f_w the fraction of the thickness immersed in water. Equation 6 thus reads

$$I_1 = I_1^{\mathrm{Air/Oil}} + I_1^{\mathrm{w}} \qquad \text{(Eq. 13)}$$

with

$$I_1^{\mathrm{Air/Oil}} = \frac{\left(n^2_{\mathrm{protAir/Oil}} - n^2_{\mathrm{Air/Oil}}\right)\left(n^2_{\mathrm{protAir/Oil}} - n^2_{\mathrm{bulk}}\right)}{n^2_{\mathrm{protAir/Oil}}} (1- f_w)\, H \qquad \text{(Eq. 14)}$$

and

$$I_1^{\mathrm{w}} = \frac{\left(n^2_{\mathrm{protsolv}} - n^2_{\mathrm{Air/Oil}}\right)\left(n^2_{\mathrm{protsolv}} - n^2_{\mathrm{bulk}}\right)}{n^2_{\mathrm{protsolv}}} f_w H \qquad \text{(Eq. 15)}$$

Here, $n_{\mathrm{Air/Oil}}$ is the index of refraction of air or oil depending on the interface considered, n_{bulk} is the index of refraction of the bulk aqueous phase, as measured experimentally (Fig. SI1d in supplementary information). $n_{\mathrm{protAir/Oil}}$, respectively n_{protsolv}, is the index of refraction of the protein layer in air or oil, respectively in the aqueous solvent. Following Eq. 2,

$$n^2_{\text{protAir/Oil}} = n^2_{\text{Air/Oil}} + \phi_P\,(n^2_{\text{prot}} - n^2_{\text{Air/Oil}}) \quad \text{(Eq. 16)}$$

and

$$n^2_{\text{protsolv}} = n^2_{\text{solv}} + \phi_P\,(n^2_{\text{prot}} - n^2_{\text{solv}}) \quad \text{(Eq. 17)}$$

with ϕ_P the volume fraction of proteins in the interfacial layer which is related to the surface excess concentration using:

$$\phi_P = \frac{\Gamma}{\rho_P H} \quad \text{(Eq. 18)}$$

with ρ_P the protein mass density.

Using Eqs. 13-18, we can compute the sets of parameters (H, f_w) which are compatible with the experimental values of I_1 measured at the air-water interface in the three regimes of adsorption. In regime I, at the beginning of adsorption ($0 < I_1 < 0.17$ nm) we assume $\Gamma = 1$ mg/m² < Γ_{mf}; in the pseudo-plateau regime II ($0.37 < I_1 < 0.45$ nm) we use the saturation value estimated previously $\Gamma_{mf} = 2.8$ mg/m² and in regime III ($0.8 < I_1 < 0.45$ nm), we consider $\Gamma = 6$ mg/m² (very close to $\Gamma_{mf} + \Gamma_{ms}$). In the case of the air/water interface, and for all regimes, we find that only films mainly in the aqueous phase ($f_w > 0.7$) would give numerical values compatible with the experimental ones (Fig. 7a). By contrast, at the oil-water interface (Fig. 7b), using the same hypothetic surface excess concentrations at the beginning of adsorption ($\Gamma = 1$ mg/m²) and in the pseudo plateau regime ($\Gamma_{mf} = 2.8$ mg/m²), the experimental values measured are expected for films mainly in the organic phase ($f_w < 0.3$). Interestingly, in the last regime, considering a further adsorption ($\Gamma = 6$ mg/m²), only thick films ($H > 10$ nm) mainly in the aqueous phase ($f_w > 0.4$) can account for the experimental negative values of the ellipsometric signal.

To summarize, at the air-water interface, the interfacial film would be mainly formed in the aqueous phase whatever the adsorption regime. The formation of the protein interfacial film is kinetically controlled by the diffusion of the two populations of species identified in the bulk. By contrast, at the oil water-interface, proteins would initially adsorb mainly on the oil side of the interface and the film would later grow in the aqueous phase concomitantly to the adsorption of the large objects present in the bulk.

Long ageing time regime

In addition, as mentioned above, for large bulk concentrations ($C \geq 10$ g/L) and long ageing times ($t \geq 1$ h), the Brewster angles are significantly different from the ones of the bare interfaces and

the perturbation theory is no more valid (see Fig. SI2 in supplementary information). A few multi-angle ellipsometry experiments are performed at the air-water interface in this regime. We measure the evolution of the angles Δ and Ψ as a function of the incident angle, for a bulk concentration C=10 g/L at two ageing times (1 and 60 hours) (Fig. 8). We find that the position of the minimum of tan Ψ, associated to the Brewster angle, shifts from 53.3 deg. to 55.1 deg. with ageing time (bare interface 53.2 deg.) and the minimum of tan Ψ becomes sharper. Data are nicely fitted using the stratified layer model using one average layer for the film. The fitting parameters (n_L and H) are given in Table 1 for the two ageing times. After 1 hour of adsorption the estimated film thickness (H = 15 nm) is fully consistent with the equivalent radius, R_{eq} = 7.5 nm, defined from the saturation excess concentration of the monolayer, Γ_{mf}, and corresponds to a protein monolayer of protein hexamers. After 60 hours the film thickness (H = 130 nm) is by contrast comparable to the size of the large objects identified in the bulk protein suspension ($R_{H,s}$ = (77 ± 10) nm). Based on the analysis of the evolution of I_1 at the air-water interface for shorter ageing times, we suppose an interfacial protein film exclusively in the aqueous phase. From the fitting parameters, n_L and H, considering the interfacial layer made of solvated protein ($\mathrm{n_L} = \mathrm{n_{protsolv}}$), we can evaluate the protein volume fraction in the film Φp (Eq. 17) and the surface excess concentration Γ (Eq. 18). From 1 h to 60 h of ageing time, $\Phi p \sim 0.3$ is constant suggesting a constant film organization, while the film thickness drastically increases from 15 to 130 nm. Unfortunately, no similar data can be acquired for the oil-water interface as optical measurements at this interface are instable over such long ageing times.

Besides, in the long ageing time regime we observe that aqueous drops formed during pendant drop tensiometry measurements become turbid (Fig. 9). From the difference in the grey level for the drop and for the neck of the drop (see e.g. pictures acquired at t_2 and t_3 in Fig. 9), we can deduce that the turbidity could not uniquely originate from differences in the liquid/liquid interface but should also be present in the bulk of the drop. We quantify the decrease of transparency by a normalized grey level of the drop images:

$$P_X^N = \frac{P_X(t)D(0)}{D(t)P_X(0)} \qquad \text{(Eq. 19)}$$

Here $Px(t)$ *is* the average grey level of the yellow disc of constant radius (see Fig. 9a) and $D(t)$ is the maximum lateral dimension of the image of the drop acquired at time t (with t=0 for the first picture acquired just after the formation of a drop). The decrease of transparency is observed before

30 minutes for protein solutions at 10 g/L whatever the interface while it is only observed at the oil-water interface after 2 hours of adsorption for C = 1 g/L. Consequently, the increase of turbidity of the drop appears promoted by the protein concentration and more pronounced for an oil-water interface than for an air-water interface. In addition, interestingly, when the drop is detached and a new drop is formed from the same bulk solution stored in the same conditions as the previous drop, the fresh drop is perfectly transparent (large empty symbols in Fig. 9b). This unambiguously demonstrates that the bulk turbidity is not formed directly in the bulk but is instead induced by the liquid interfaces of the drop. Hence from these observations we suggest that the large objects that are responsible for the turbidity increase would detach from interfaces that promote aggregation of the protein extract.

3.2 Discussion

Sunflower proteins and complexes

Dynamic light scattering experiments show, for a sunflower protein isolate dispersed in good solvent conditions, the coexistence of two diffusive populations of contrasted sizes in the bulk. The small objects (hydrodynamic radius ~6 nm) are presumably the hexameric form of globulins. The large objects (hydrodynamic radius ~77 nm), on the other hand, are in minor proportion by weight as compared to the small objects. They display an internal dynamic, implying that these large objects have a low density. We suggest that the large objects are complexes, which could form between globulins and chlorogenic acid, since phenolic compounds absorbing at 325 nm appear co-eluted with proteins in SE-HPLC (see Fig. SI1a of the supplementary information). The nature of the interactions involved in these complexes is not known. According to the literature such complexes would be covalent in alkaline conditions, while non-covalent hydrogen bonds would be involved at neutral pH[3]. Sunflower protein-chlorogenic acids complexes of typical size 100 nm have been shown to form at neutral pH[23], seemingly consistent with our measurements, although our measurements are performed in alkaline medium and in presence of much less chlorogenic acid. We are not aware of previous measurements of the size of covalent complexes which are known to give a green color to solutions.

A three-step adsorption mechanism

We investigate the adsorption of the protein isolate at the air-water and oil-water interfaces using tensiometry, dilational rheology and ellipsometry. We have shown that data acquired at different bulk isolate concentrations can be recast into master curves (Fig. 2-4). Building master curves is a common approach to investigate how the dilational elasticity varies with the surface pressure upon adsorption of proteins at liquid interfaces[47]. To the best of our knowledge, using time-concentration superposition to rationalize the time evolution of the surface pressure was only attempted in the initial adsorption regime for proteins[48] before we recently provide experimental evidence that time-concentration superposition holds during the whole duration of the adsorption of a soft plant protein at a liquid/liquid interface[37]. Here, the master curves (Figs. 2, 3) unambiguously highlight three adsorption regimes, which are summarized in the scheme of Figure 10: the initial diffusive adsorption (regime I), the monolayer saturation (regime II) and the additional adsorption of complexes (regime III).

Regime I, which corresponds to the initial regime of adsorption, is evidenced with data acquired with small bulk concentrations ($C < 0.1$ g/L) and at short times. Time-concentration superposition holds for all kinds of data, as evidenced with the master curve representations (Figs. 2c, 3, 4c, d). Using tensiometry, this regime is characterized by a lag-time followed by a steep increase of the surface pressure with time. The time-shifting factors, α, used to plot master curves (Fig. 2d) follow an evolution characteristic of diffusion-controlled processes[37], in full accordance with ellipsometric data that display the characteristic power law evolution of the surface excess concentration as a function of time for a diffusion-controlled adsorption, $\Gamma \propto t^{1/2}$. The initial diffusive adsorption has been previously described in the literature for sunflower proteins[49]. Previous works on lyzozyme suggest an adsorption barrier associated to the very high conformational stability of this protein[4]. In our case we do not have any hint of an adsorption barrier which is consistent with the intermediate instability index *II* of sunflower globulins (*II*=57.45). This index is comprised between those of globular proteins such that lysozyme (*II*=20.93), β-lactoglobulin (*II*=40.12), BSA (*II*=41.56) and those of more disordered proteins such as β-casein (*II*=96.62) or γ-gliadin (II=109.79)[1]. Besides, the linear relation of the dilational elastic moduli to the surface pressure associated with a large proportionality constant is typical for hard proteins (β-lactoglobulin,

[1] Instability indexes were computed using the ProtParam tool of Expasy

ovalbumin)[9]. An analysis in the framework of Flory exponents suggests that the proportionality constants are consistent with the formation of 2-dimensional proteins films. This would imply an unfolding of the tertiary structure of the proteins.

In regime II, the surface pressure and the surface excess concentration reach "pseudo-plateau" values. From the surface excess concentration at the plateau (2.8 mg/m²) one can evaluate an equivalent radius for the proteins at saturation, of the order of 7.5 nm. This numerical value is close to the native radius of the proteins in the bulk, thus suggesting limited conformational changes upon adsorption. Such findings are in sharp contrast with results for a flexible protein such as wheat gliadin because of surface pressure-induced conformation changes (unpublished data). Nevertheless, in regime II we measure that the viscous moduli reach maximum values indicating a reorganization of the film at interfaces, as previously observed for β-lactoglobulin[50]. In addition, the elastic moduli continue to increase with surface pressure in this regime, with proportionality constants that indicate 3-dimensional structures for the interfacial films. These two last features could be precursors of the last regime.

The last regime, regime III, is characterized by a loss of validity of the different master curves. Such violation means that the film properties become history-dependent due to the dynamics of reorganization processes at the interface that are comparable to, or slower than, the adsorption dynamics. Recently, Fainerman et al.[51] showed deviations from the visco-elastic master curve at high concentrations, which were attributed to the flexibility of β-casein. In parallel, Ulaganathan et al.[52] interpreted similar phenomena, observed for the globular β-lactoglobulin, to protein aggregation. Interestingly, in our case, the last regime corresponds to a second increase of the surface excess concentration that can be well fitted considering that the population of complexes identified in bulk adsorb also at interfaces. Because complexes are much larger than hexamers they should adsorb later, when the monolayer of hexamers is already formed. A thick film would be thus formed in the aqueous phase with a thickness of several hundreds of nanometers according to ellipsometry. The protein volume fraction in the thick film was estimated as $\Phi p \sim 0.3$. This value corresponds to a quite dense protein film since it roughly corresponds to the density of a saturated monolayer. This density contrasts with that of the complexes probed in the bulk, which we think would be at the origin of the formation of the thick interfacial layer. However, the protein volume fraction could be overestimated if phenol compounds enter in the composition of the thick layer since the index of refraction of polyphenol (n_{phenol} = 1.6-1.7) is much larger than the one of proteins

(n_{prot} = 1.5). Our understanding of regime III in terms of adsorption of complexes is supported by the measurements of Karefyllakis et al. who showed that samples including chlorogenic acid-protein complexes display the same adsorption dynamics as the pure protein extract at short time but a further adsorption at longer time[23]. The low density polymeric structure of the complexes could induce the formation of a plastic layer; this would explain why the film does not become brittle as expected for an aggregated layer. We note that such cohesive layer could be at the origin of bridging of droplets in emulsions and could explain their good stability[23]. At very long time, the bulk solution may become turbid, but only for samples with large surface/volume ratio, because of the release of large objects from interfaces. Since polyphenols are recognized for their inhibitory action on protein aggregation into insoluble amyloid fibrils through the stabilization of small oligomers[53], the formation of aggregates in bulk induced by interfaces could be attributed to a modification of the adsorbed protein interactions in favor of the formation of stable protein aggregates in bulk with the adsorption of polyphenols.

Air-water vs oil-water interface

Qualitatively, the adsorption behavior of the sunflower isolate appears analogous at the air-water and the oil-water interfaces, as evidenced by similar macroscopic observations (Fig. 9), and by the similar shapes for the two interfaces of the master curves built using tensiometry and dilational rheology (Figs. 2c and 3). The qualitative similarity of adsorption mechanisms at air-water and oil-water interfaces was previously pointed out for microgels[54] and for model animal proteins [4-5, 7, 9, 55-56]. We nevertheless have identified some distinctive quantitative features that depend on the nature of the interface. First, the induction time measured by tensiometry is shorter at the oil-water than at the air-water interface. This was observed for most proteins previously investigated in the literature and attributed to a higher degree of unfolding of proteins at the oil-water interface due to the better solvent quality of oil for the hydrophobic amino acid side chains[4, 56-57]. In our case, such interpretation is supported by the initial proportionality constant, *p*, between the elasticity modulus and the surface pressure. We find that *p* is higher at the air-water interface than at the oil-water interface. This is consistent with a better solvent quality of oil relative to air according to the Flory-like scaling law approach. In addition, using the interfacial tensions measured at saturation, it is possible to theoretically predict the location and the behavior of proteins at different oil-water interfaces considering proteins as soft particles and assuming that the saturation correspond to an

equilibrium state for the protein[58] . Using our measurements, we can compute γ_{wp}/γ_{ow} and γ_{op}/γ_{ow} with γ_{wp} the surface tension of the air-water interface with protein at saturation (γ_{wp} = 57 mN/m), γ_{op} the surface tension of the oil-water interface with protein at saturation (γ_{op} = 25 mN/m), and γ_{ow} the surface tension of the bare oil-water interface (γ_{ow} =47 mN/m). We find γ_{wp}/γ_{ow} = 1.2 and γ_{op}/γ_{ow} = 0.53. This set of values is predicted to correspond to soft particles weakly deformed at an oil-water interface, and located mainly in the oil phase[58]. The partial location of the proteins in the oil phase is also strongly supported by ellipsometric data. Measurements at the oil-water interface are very delicate and weakly contrasted, but a careful data analysis of regimes I and II clearly shows that proteins are mainly in the oil phase once adsorbed at the hexadecane-water interface, whereas they are mainly located in the aqueous phase if adsorbed at an air-water interface. This conclusion is consistent with previous comparative neutron reflectivity studies for the location of globular proteins (BSA and β-lactoglobulin) at air-water and oil-water interfaces[59-60]. In addition, values of the dilational elastic modulus and the surface pressure measured at hexadecane-water interface (γ_{ow}=47 mN/m) at the pseudo-plateau (which corresponds to the monomeric protein saturation) are consistent with the general tendencies of evolution of these characteristic values at infinite time for globular proteins with different oil hydrophobicities[60-61]. However, note that the elastic modulus measured (E'~40mN/m) is a little bit weaker than the general tendency and can be understood considering the high instability index (II) of sunflower globulin compared to other classically investigated globular proteins.

In the last regime, the protein film expands in the aqueous phase at both interfaces and objects are released in the bulk more rapidly from the oil-water than from the air-water interface. The anchorage of the thick layer of complexes on the protein monolayer could be thus influenced by the conformation of the proteins in the interfacial monolayer.

4. Conclusion

We have investigated the interfacial properties of a sunflower extract as a first attempt to rationalize foams and emulsions with plant proteins. The interfacial properties of the sunflower proteins extract investigated here display original features compared to most pure and/or model animal proteins investigated in the literature. At short adsorption time, the sunflower extract behaves like

moderately hard proteins and a saturated monolayer is formed with a partition of proteins in the two phases that depends on the nature of the hydrophobic phase (air or oil). However, at long adsorption time, a thick layer is formed in the aqueous phase. The dynamics of formation of this layer is compatible with the adsorption of protein-polyphenol complexes which are initially dispersed in the bulk and suggests a synergic effect of proteins and phenolic compounds in the stabilization of interfaces. It is in line with studies that show a better stability of emulsions stabilized with protein isolate in the presence of moderate amounts of chlorogenic acid[62]. As a consequence, in addition to their anti-oxidant properties[63], polyphenolic compounds could be used to modulate stabilization properties of proteins. As these compounds coexist with proteins in plants, and are moreover difficult to remove, the use of less pure extracts obtained with mild processes appears interesting[64]. A dedicated study of the impact of controlled quantities of polyphenols in protein extract on the interfacial properties would be required in the future.

Supporting information

Figure 1: a) SE-HPLC profile of the sunflower protein extract – b) pH dependent solubility of the extract – c) DSC thermogram of the extract – d) Refractive index of protein solutions

Figure 2: Brewster angle variations with protein solutions at different concentrations

Acknowledgments

This work was performed, in partnership with the SAS PIVERT, within the frame of the French Institute for the Energy Transition (ITE P.I.V.E.R.T., www.institut-pivert.com) selected as an Investment for the Future by the French Government under the reference ANR-001-01.A. Banc thank the French National Agency for Research (ANR 18 CE06 001201) for teaching discharge. The authors thank Sara Albe Slabi and Odile Messieres for the extraction and the biochemical characterization of sunflower proteins.

References

1. Sá, A. G. A.; Moreno, Y. M. F.; Carciofi, B. A. M., Plant proteins as high-quality nutritional source for human diet. *Trends in Food Science & Technology* **2020,** *97*, 170-184.
2. Can Karaca, A.; Low, N. H.; Nickerson, M. T., Potential use of plant proteins in the microencapsulation of lipophilic materials in foods. *Trends in Food Science & Technology* **2015,** *42* (1), 5-12.
3. Wildermuth, S. R.; Young, E. E.; Were, L. M., Chlorogenic Acid Oxidation and Its Reaction with Sunflower Proteins to Form Green-Colored Complexes. *Comprehensive Reviews in Food Science and Food Safety* **2016,** *15* (5), 829-843.
4. Mitropoulos, V.; Mutze, A.; Fischer, P., Mechanical properties of protein adsorption layers at the air/water and oil/water interface: A comparison in light of the thermodynamical stability of proteins. *Adv Colloid Interfac* **2014,** *206*, 195-206.
5. Beverung, C. J.; Radke, C. J.; Blanch, H. W., Protein adsorption at the oil/water interface: characterization of adsorption kinetics by dynamic interfacial tension measurements. *Biophys Chem* **1999,** *81* (1), 59-80.
6. Graham, D. E.; Phillips, M. C., Proteins at Liquid Interfaces .1. Kinetics of Adsorption and Surface Denaturation. *Journal of colloid and interface science* **1979,** *70* (3), 403-414.
7. Graham, D. E.; Phillips, M. C., Proteins at liquid interfaces: II. Adsorption isotherms. *Journal of colloid and interface science* **1979,** *70* (3), 415-426.
8. Cicuta, P.; Hopkinson, I., Studies of a weak polyampholyte at the air-buffer interface: The effect of varying pH and ionic strength. *J Chem Phys* **2001,** *114* (19), 8659-8670.
9. Lucassen-Reynders, E. H.; Benjamins, J.; Fainerman, V. B., Dilational rheology of protein films adsorbed at fluid interfaces. *Curr Opin Colloid In* **2010,** *15* (4), 264-270.
10. Yano, Y. F.; Arakawa, E.; Voegeli, W.; Kamezawa, C.; Matsushita, T., Initial Conformation of Adsorbed Proteins at an Air–Water Interface. *The Journal of Physical Chemistry B* **2018,** *122* (17), 4662-4666.
11. Guruprasad, K.; Reddy, B. V. B.; Pandit, M. W., Correlation between stability of a protein and its dipeptide composition: a novel approach for predicting in vivo stability of a protein from its primary sequence. *Protein Engineering, Design and Selection* **1990,** *4* (2), 155-161.
12. Lomascolo, A.; Uzan-Boukhris, E.; Sigoillot, J. C.; Fine, F., Rapeseed and sunflower meal: a review on biotechnology status and challenges. *Applied Microbiology and Biotechnology* **2012,** *95* (5), 1105-1114.
13. Gonzalez-Perez, S.; Vereijken, J. M., Sunflower proteins: overview of their physicochemical, structural and functional properties. *Journal of the Science of Food and Agriculture* **2007,** *87* (12), 2173-2191.
14. Kortt, A. A.; Bruce Caldwell, J., Sunflower 11S globulin, susceptibility to proteolytic cleavage of the subunits of native helianthinin during isolation: HPLC fractionation of the subunits. *Phytochemistry* **1990,** *29* (5), 1389-1396.
15. Kortt, A. A.; Caldwell, J. B., Low-Molecular-Weight Albumins from Sunflower Seed - Identification of a Methionine-Rich Albumin. *Phytochemistry* **1990,** *29* (9), 2805-2810.
16. Plietz, P.; Damaschun, G.; Muller, J. J.; Schwenke, K.-D., The Structure of 11-S Globulins from Sunflower and Rape Seed. *European Journal of Biochemistry* **1983,** *130* (2), 315-320.
17. Gonzalez-Perez, S.; Vereijken, J. M.; Merck, K. B.; Van Koningsveld, G. A.; Gruppen, H.; Voragen, A. G. J., Conformational states of sunflower (Helianthus annuus) helianthinin: Effect of heat and pH. *Journal of agricultural and food chemistry* **2004,** *52* (22), 6770-6778.

18. Dalgalarrondo, M.; Raymond, J.; Azanza, J.-L., Sunflower Seed Proteins: Characterization and Subunit Composition of the Globulin Fraction. *Journal of experimental botany* **1984,** *35* (11), 1618-1628.
19. Gonzalez-Perez, S.; van Konigsveld, G. A.; Vereijken, J. M.; Merck, K. B.; Gruppen, H.; Voragen, A. G., Emulsion properties of sunflower (Helianthus annuus) proteins. *Journal of agricultural and food chemistry* **2005,** *53* (6), 2261-7.
20. Gonzalez-Perez, S.; Vereijken, J. M.; van Koningsveld, G. A.; Gruppen, H.; Voragen, A. G., Formation and stability of foams made with sunflower (Helianthus annuus) proteins. *Journal of agricultural and food chemistry* **2005,** *53* (16), 6469-76.
21. Defaix, C.; Aymes, A.; Albe Slabi, S.; Basselin, M.; Mathé, C.; Galet, O.; Kapel, R., A new size-exclusion chromatography method for fast rapeseed albumin and globulin quantification. *Food chemistry* **2019,** *287*, 151-159.
22. Albe Slabi, S.; Mathé, C.; Framboisier, X.; Defaix, C.; Mesieres, O.; Galet, O.; Kapel, R., A new SE-HPLC method for simultaneous quantification of proteins and main phenolic compounds from sunflower meal aqueous extracts. *Analytical and Bioanalytical Chemistry* **2019,** *411* (10), 2089-2099.
23. Karefyllakis, D.; Altunkaya, S.; Berton-Carabin, C. C.; van der Goot, A. J.; Nikiforidis, C. V., Physical bonding between sunflower proteins and phenols: Impact on interfacial properties. *Food Hydrocolloids* **2017,** *73*, 326-334.
24. Fischer, H.; Polikarpov, I.; Craievich, A. F., Average protein density is a molecular-weight-dependent function. *Protein Science* **2004,** *13* (10), 2825-2828.
25. Gekko, K.; Hasegawa, Y., Compressibility-structure relationship of globular proteins. *Biochemistry* **1986,** *25* (21), 6563-6571.
26. Aspnes, D. E., Optical-Properties of Thin-Films. *Thin Solid Films* **1982,** *89* (3), 249-262.
27. Berry, J. D.; Neeson, M. J.; Dagastine, R. R.; Chan, D. Y. C.; Tabor, R. F., Measurement of surface and interfacial tension using pendant drop tensiometry. *Journal of colloid and interface science* **2015,** *454*, 226-237.
28. Loglio, G. P., P.; Miller, R.; Makievski, A.V.; Ravera, F.; Ferrari, M.; Liggieri, L., Drop and bubble shape analysis as tool for dilatational rheology of interfacial layers. In *Novel Methods to Study Interfacial Layers*, D. Möbius, R. M., Ed. Elsevier: 2001.
29. Lekner, J., *Theory of Reflection*. Springer Netherlands: Dordrecht, The Netherlands, 1987.
30. Azzam, R. M. A.; Bashara, N. M., *Ellipsometry and Polarized Light*. North-Holland Publishing Company: 1977.
31. Trappe, V.; Bauer, J.; Weissmüller, M.; Burchard, W., Angular Dependence in Static and Dynamic Light Scattering from Randomly Branched Systems. *Macromolecules* **1997,** *30* (8), 2365-2372.
32. Yang, C.; Meng, B.; Chen, M.; Liu, X.; Hua, Y.; Ni, Z., Laser-light-scattering study of structure and dynamics of waxy corn amylopectin in dilute aqueous solution. *Carbohydrate Polymers* **2006,** *64* (2), 190-196.
33. Dahesh, M.; Banc, A.; Duri, A.; Morel, M. H.; Ramos, L., Polymeric Assembly of Gluten Proteins in an Aqueous Ethanol Solvent. *J Phys Chem B* **2014,** *118* (38), 11065-11076.
34. Dubois-Violette, E.; de Gennes, P. G., Quasi-elastic scattering by dilute, ideal, polymer solutions: II. Effects of hydrodynamic interactions. *Physics Physique Fizika* **1967,** *3* (4), 181-198.
35. Shibayama, M.; Karino, T.; Okabe, S., Distribution analyses of multi-modal dynamic light scattering data. *Polymer* **2006,** *47* (18), 6446-6456.
36. Flory, P. J., *Principles in Polymer Chemistry*. Cornell University Press: Ithaca 1953.
37. Poirier, A.; Banc, A.; Stocco, A.; In, M.; Ramos, L., Multistep building of a soft plant protein film at the air-water interface. *Journal of colloid and interface science* **2018,** *526*, 337-346.
38. Daoud, M.; De Gennes, P. G., Statistics of macromolecular solutions trapped in small pores. *J. Phys. France* **1977,** *38* (1), 85-93.

39. Douillard, R.; Daoud, M.; Aguie-Beghin, V., Polymer thermodynamics of adsorbed protein layers. *Curr Opin Colloid In* **2003,** *8* (4-5), 380-386.
40. Toomey, R.; Mays, J.; Tirrell, M., In Situ Thickness Determination of Adsorbed Layers of Poly(2-Vinylpyridine)−Polystyrene Diblock Copolymers by Ellipsometry. *Macromolecules* **2004,** *37* (3), 905-911.
41. Ramirez, P.; Stocco, A.; Munoz, J.; Miller, R., Interfacial rheology and conformations of triblock copolymers adsorbed onto the water-oil interface. *Journal of colloid and interface science* **2012,** *378*, 135-143.
42. Stocco, A.; Tauer, K.; Pispas, S.; Sigel, R., Dynamics of amphiphilic diblock copolymers at the air-water interface. *Journal of colloid and interface science* **2011,** *355* (1), 172-178.
43. Miura, T.; Seki, K., Diffusion Influenced Adsorption Kinetics. *J Phys Chem B* **2015,** *119* (34), 10954-10961.
44. Douglas, J. F.; Johnson, H. E.; Granick, S., A Simple Kinetic-Model of Polymer Adsorption and Desorption. *Science* **1993,** *262* (5142), 2010-2012.
45. Pezennec, S.; Gauthier, F.; Alonso, C.; Graner, F.; Croguennec, T.; Brule, G.; Renault, A., The protein net electric charge determines the surface rheological properties of ovalbumin adsorbed at the air-water interface. *Food Hydrocolloids* **2000,** *14* (5), 463-472.
46. van Vliet, T.; Martin, A. H.; Bos, M. A., Gelation and interfacial behaviour of vegetable proteins. *Curr Opin Colloid In* **2002,** *7* (5), 462-468.
47. Benjamins, J.; Cagna, A.; LucassenReynders, E. H., Viscoelastic properties of triacylglycerol/water interfaces covered by proteins. *Colloid Surface A* **1996,** *114*, 245-254.
48. Ybert, C.; di Meglio, J. M., Study of protein adsorption by dynamic surface tension measurements: Diffusive regime. *Langmuir : the ACS journal of surfaces and colloids* **1998,** *14* (2), 471-475.
49. Rodríguez Patino, J. M.; Miñones Conde, J.; Linares, H. M.; Pedroche Jiménez, J. J.; Carrera Sánchez, C.; Pizones, V.; Rodríguez, F. M., Interfacial and foaming properties of enzyme-induced hydrolysis of sunflower protein isolate. *Food Hydrocolloids* **2007,** *21* (5), 782-793.
50. Ulaganathan, V.; Retzlaff, I.; Won, J. Y.; Gochev, G.; Gehin-Delval, C.; Leser, M.; Noskov, B. A.; Miller, R., beta-Lactoglobulin adsorption layers at the water/air surface: 1. Adsorption kinetics and surface pressure isotherm: Effect of pH and ionic strength. *Colloid Surface A* **2017,** *519*, 153-160.
51. Fainerman, V. B.; Kovalchuk, V. I.; Aksenenko, E. V.; Zinkovych, I. I.; Makievski, A. V.; Nikolenko, M. V.; Miller, R., Dilational Viscoelasticity of Proteins Solutions in Dynamic Conditions. *Langmuir : the ACS journal of surfaces and colloids* **2018,** *34* (23), 6678-6686.
52. Ulaganathan, V.; Retzlaff, I.; Won, J. Y.; Gochev, G.; Gunes, D. Z.; Gehin-Delval, C.; Leser, M.; Noskov, B. A.; Miller, R., beta-Lactoglobulin adsorption layers at the water/air surface: 2. Dilational rheology: Effect of pH and ionic strength. *Colloid Surface A* **2017,** *521*, 167-176.
53. Nedumpully-Govindan, P.; Kakinen, A.; Pilkington, E. H.; Davis, T. P.; Chun Ke, P.; Ding, F., Stabilizing Off-pathway Oligomers by Polyphenol Nanoassemblies for IAPP Aggregation Inhibition. *Scientific reports* **2016,** *6* (1), 19463.
54. Picard, C.; Garrigue, P.; Tatry, M.-C.; Lapeyre, V.; Ravaine, S.; Schmitt, V.; Ravaine, V., Organization of Microgels at the Air–Water Interface under Compression: Role of Electrostatics and Cross-Linking Density. *Langmuir : the ACS journal of surfaces and colloids* **2017,** *33* (32), 7968-7981.
55. Benjamins, J.; Lyklema, J.; Lucassen-Reynders, E. H., Compression/expansion rheology of oil/water interfaces with adsorbed proteins. Comparison with the air/water surface. *Langmuir : the ACS journal of surfaces and colloids* **2006,** *22*, 6181.
56. Murray, B. S., Equilibrium and dynamic surface pressure-area measurements on protein films at air-water and oil-water interfaces. *Colloids and Surfaces A: Physicochemical and Engineering Aspects* **1997,** *125* (1), 73-83.

57. Miller, R.; Krägel, J.; Wüstneck, R.; Wilde, P. J.; Li, J. B.; Fainerman, V. B.; Loglio, G.; Neumann, A. W., Adsorption kinetics and rheological properties of food proteins at air/water and oil/water interfaces. *Food / Nahrung* **1998,** *42* (03-04), 225-228.
58. Style, R. W.; Isa, L.; Dufresne, E. R., Adsorption of soft particles at fluid interfaces. *Soft matter* **2015,** *11* (37), 7412-7419.
59. Campana, M.; Hosking, S. L.; Petkov, J. T.; Tucker, I. M.; Webster, J. R. P.; Zarbakhsh, A.; Lu, J. R., Adsorption of Bovine Serum Albumin (BSA) at the Oil/Water Interface: A Neutron Reflection Study. *Langmuir : the ACS journal of surfaces and colloids* **2015,** *31* (20), 5614-5622.
60. Bergfreund, J.; Diener, M.; Geue, T.; Nussbaum, N.; Kummer, N.; Bertsch, P.; Nyström, G.; Fischer, P., Globular protein assembly and network formation at fluid interfaces: effect of oil. *Soft matter* **2021**.
61. Bergfreund, J.; Bertsch, P.; Fischer, P., Adsorption of proteins to fluid interfaces: Role of the hydrophobic subphase. *Journal of colloid and interface science* **2021,** *584*, 411-417.
62. Pan, X.; Fang, Y.; Wang, L.; Shi, Y.; Xie, M.; Xia, J.; Pei, F.; Li, P.; Xiong, W.; Shen, X.; Hu, Q., Covalent Interaction between Rice Protein Hydrolysates and Chlorogenic Acid: Improving the Stability of Oil-in-Water Emulsions. *Journal of agricultural and food chemistry* **2019,** *67* (14), 4023-4030.
63. Ozdal, T.; Capanoglu, E.; Altay, F., A review on protein–phenolic interactions and associated changes. *Food Research International* **2013,** *51* (2), 954-970.
64. Karefyllakis, D.; Octaviana, H.; van der Goot, A. J.; Nikiforidis, C. V., The emulsifying performance of mildly derived mixtures from sunflower seeds. *Food Hydrocolloids* **2019,** *88*, 75-85.

TOC Graphic

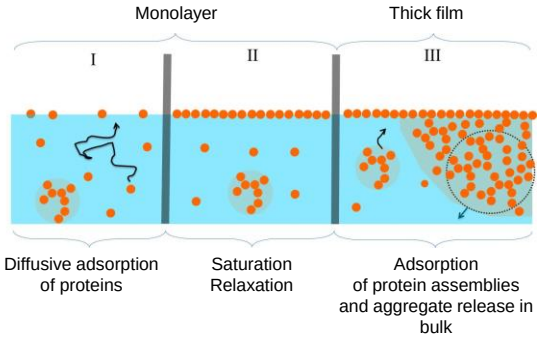
Monolayer
Thick film
I
II
III
Diffusive adsorption of proteins
Saturation Relaxation
Adsorption of protein assemblies and aggregate release in bulk

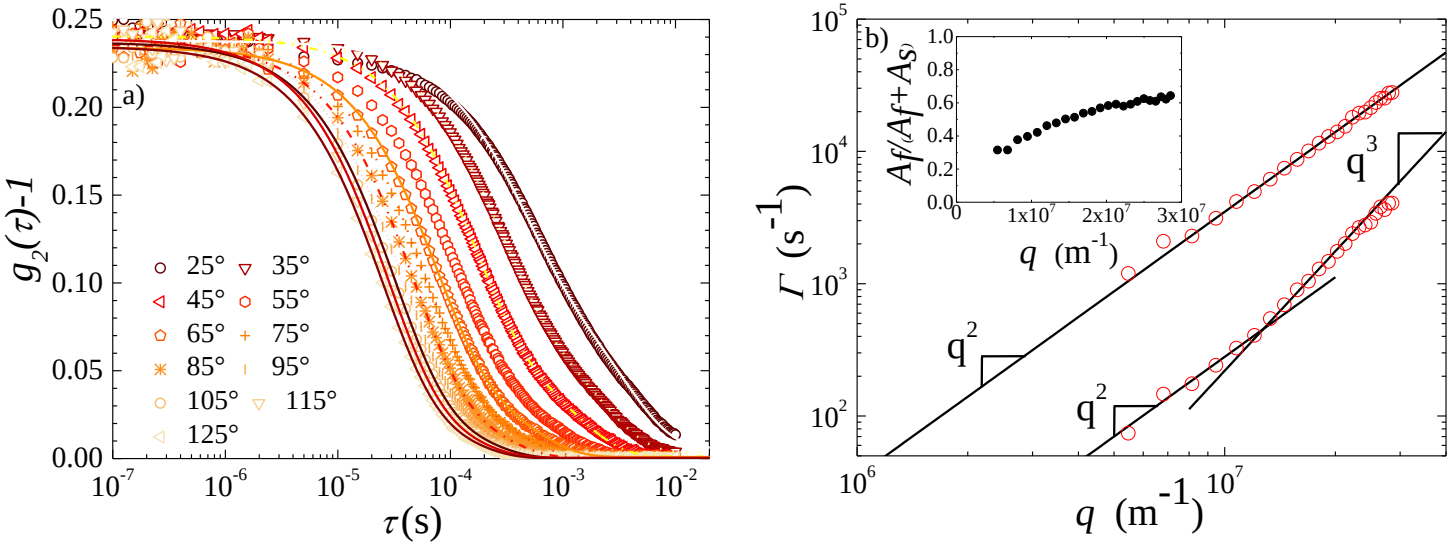

Fig. 1 (a) Dynamic light scattering: Correlation functions measured at different angles, θ, as indicated in the legend, for a sample with protein concentration C =5 g/L. The symbols are the experimental data points, and the lines are best fits with a double exponential decay functional form. (b) Decay rates as function of wavevector q. Inset: Relative amplitude of the fast contribution of the double exponential decays as a function of q.

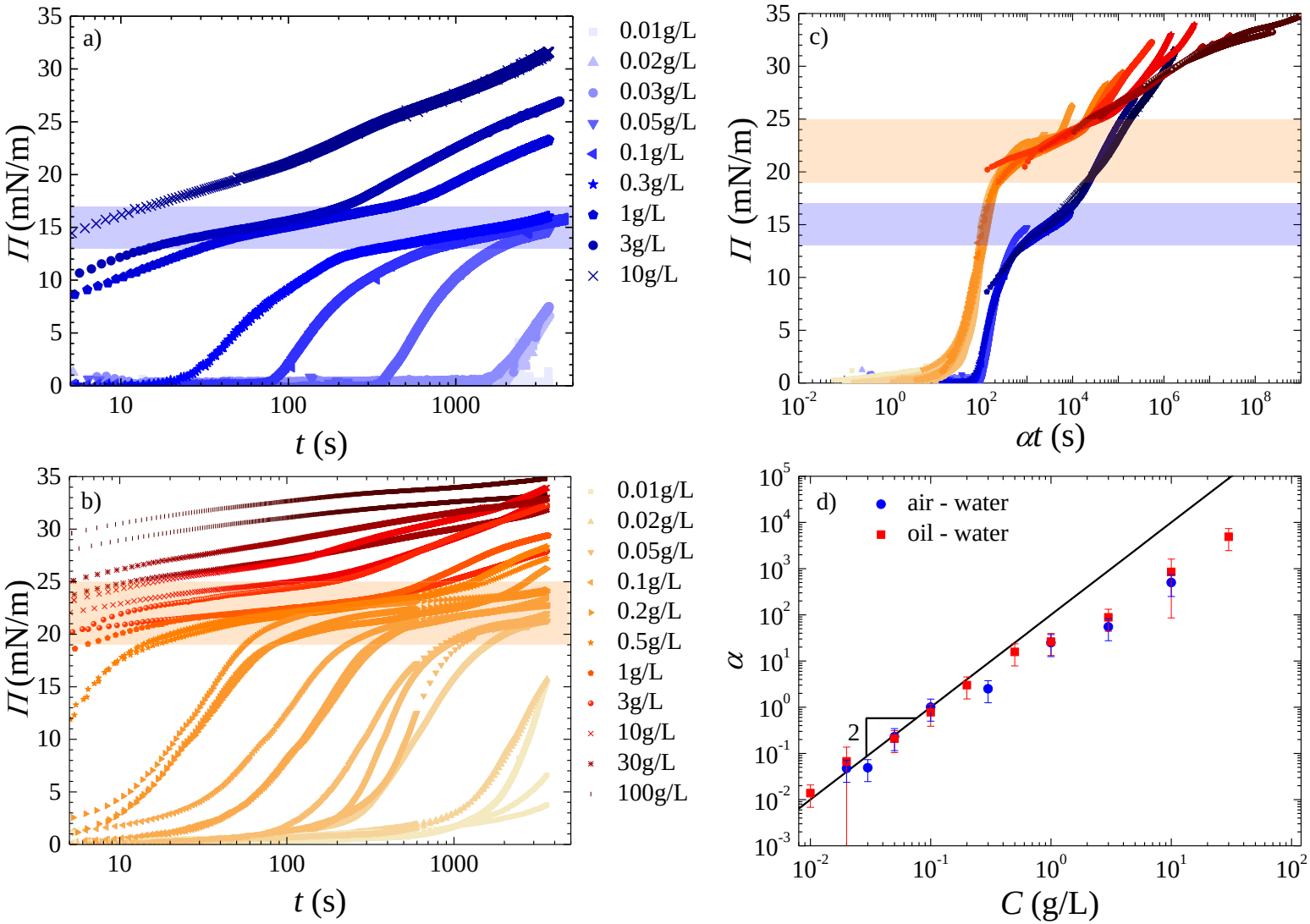

Fig. 2 Time evolution of the surface pressure Π at a) Air – water, b) Oil – water interfaces for different bulk protein concentrations, *C*, as indicated in the legend. The horizontal band defines the pseudo-plateau of the surface pressure.
c) Master curves obtained by plotting the surface pressure as a function of a normalized time, αt, using C = 0.1 g/L as reference for air-water (blue) and oil-water (red) interfaces. The horizontal bands display the pseudo-plateaus.
d) Scale factor α, as a function of bulk protein concentration. The line is the theoretical expectation for a diffusive process.

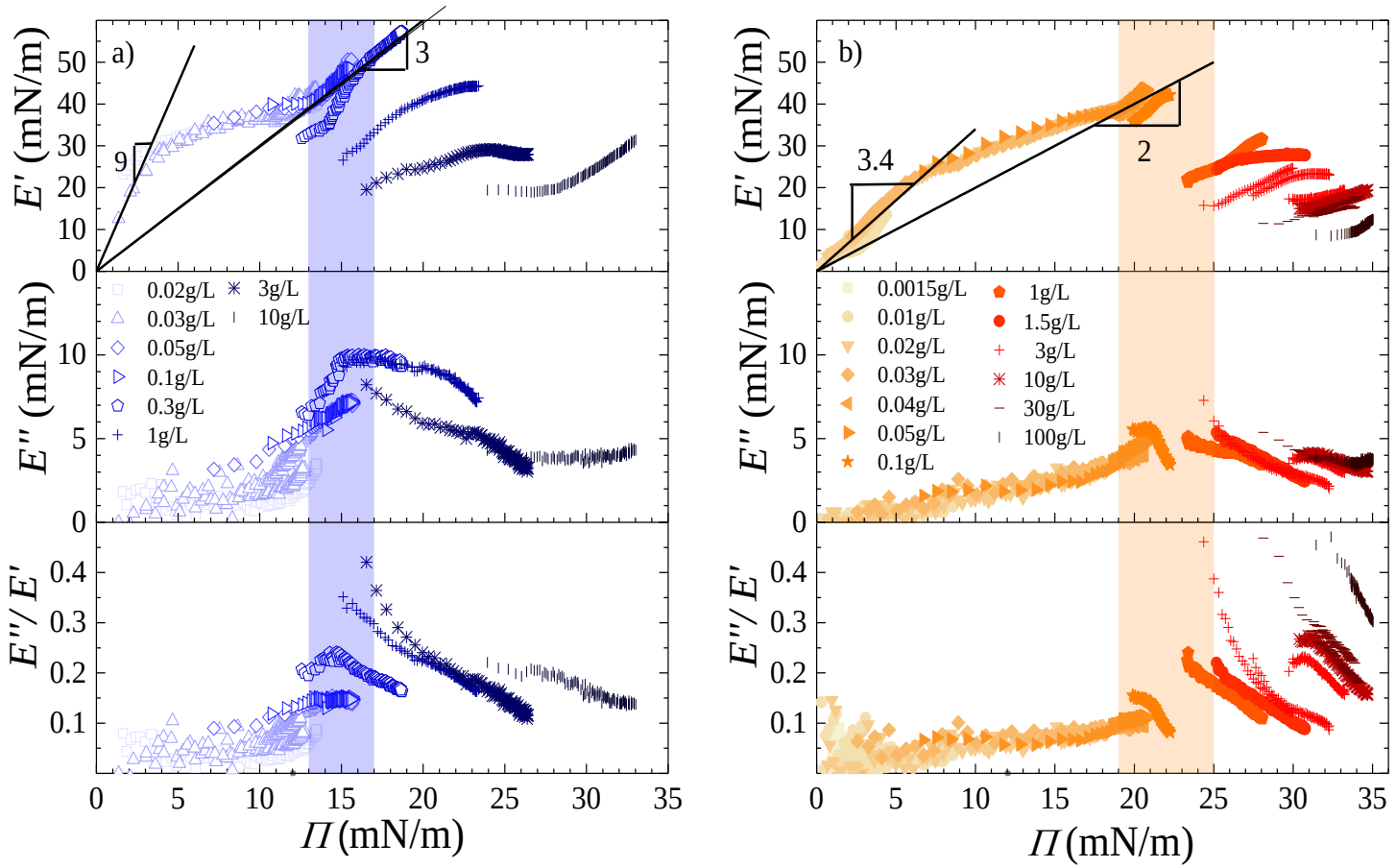

Fig. 3 Dilatational elastic modulus *E'*, viscous modulus *E"*, and ratio, *E"/E',* as a function of the surface pressure, Π, for different protein concentrations as indicated in the caption. The colored vertical bands display the surface pressure pseudo plateaus evidenced in figures 2 & 3.

a) air –water interface b) oil – water interface. The lines in the *E'* vs Π plots are linear fits of data points at low Π and in the plateau regime.

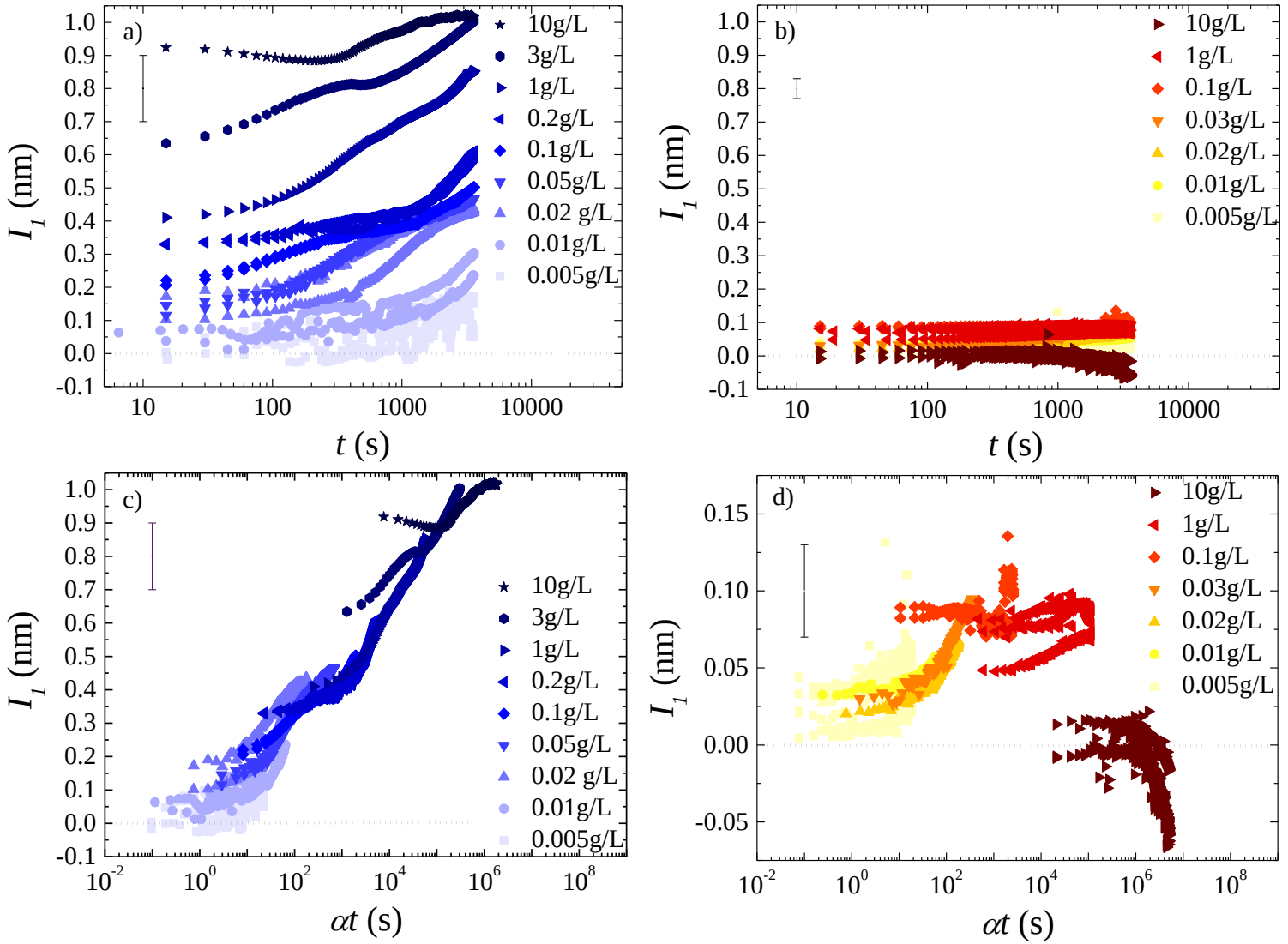

Fig. 4 Deviation parameter I_1 as a function of time t at the air – water (a) and oil – water (b) interfaces. Horizontal dashed lines show I_1=0. The same data as in (a) and (b) are plotted as a function of αt in figures (c) and (d). The experimental scaling factors α derived from fig 3.b are used. The error bars (evaluated by repetition of measurements) are constant for a given interface and are represented on the left hand side of each plot by only one bar for clarity of plots.

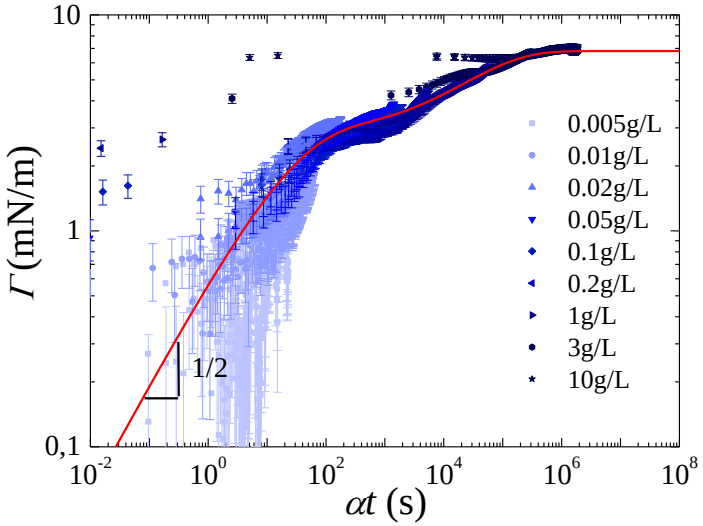

Fig. 5 Surface excess concentration at an air-water interface as a function of the normalized time αt. The thin line is the best fit of the experimental data with the diffusive model (Eq.12) using Γ_{m1} = 2.8 mg/m², Γ_{m2} = 4 mg/m² and w_s= 0.1.

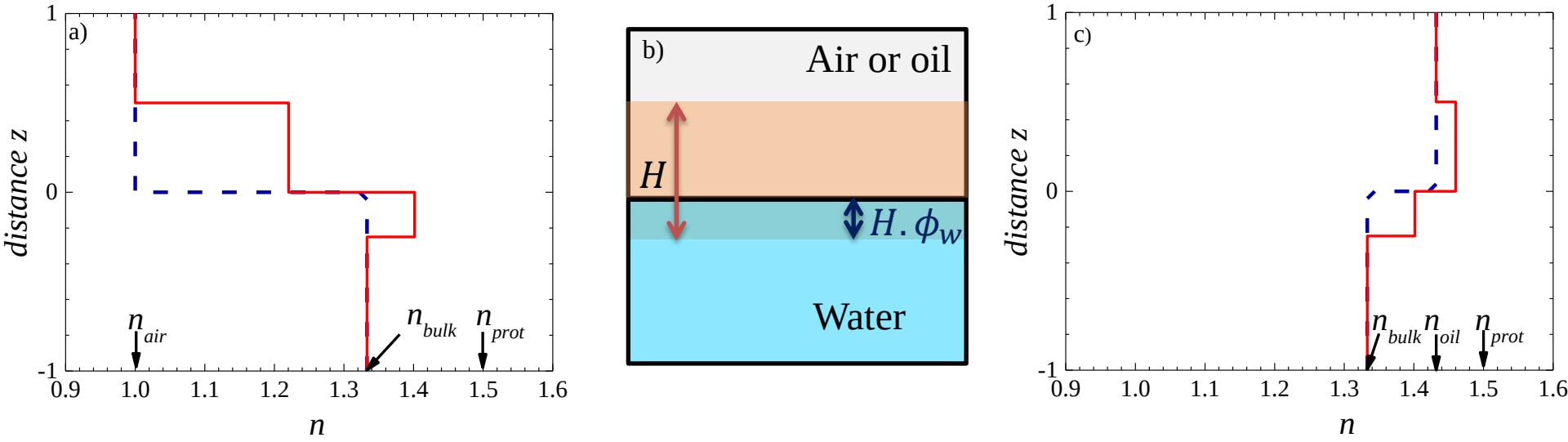

Fig. 6 (a) and (c) Refractive index profile close to the interface. The blue dashed line indicates the optical profile of an empty interface and the red line shows the optical profile of the protein film adsorbed at the interface with the proteins partially in water and partially in the second phase (air or oil). The protein volume fraction at the interface is arbitrary taken as ϕ_p = 39 %. Left: air-water Right: oil-water interfaces.
Middle: Scheme of the protein film at the interface. The protein film is symbolized by a layer of thickness *H.* The film thickness in the aqueous phase is $H.\phi_w$.

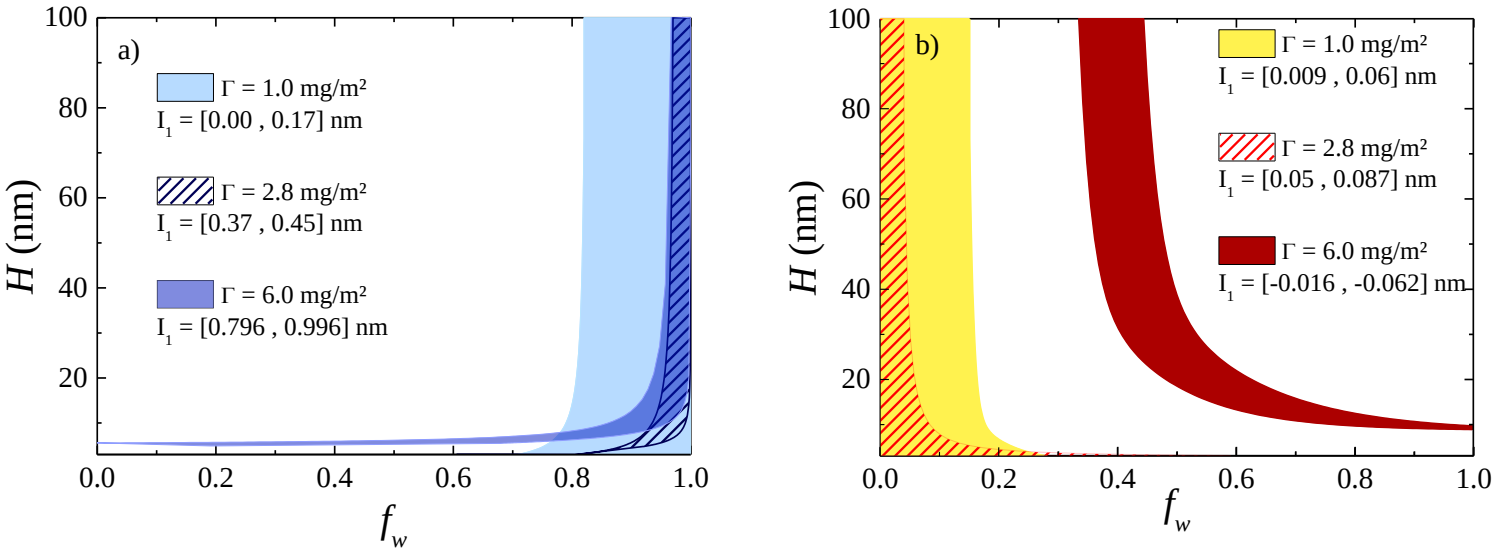

Fig. 7 Film thickness H as a function of the protein fraction in water ϕ_w. Colored and dashed area represent the couples (H , f_w) giving the experimental values for I_1 and Γ given in the legend according to equations 14 to 19, for (a) air-water (b) oil-water interfaces.

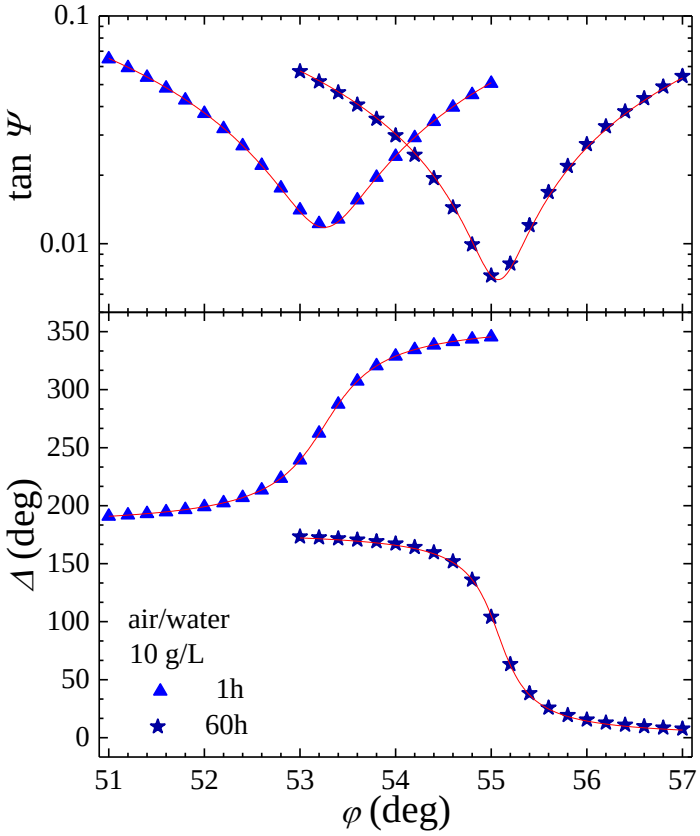

Fig.8 Ellipsometric angles, Δ and ψ, as a function of the incidence angle φ, at the air-water interface for a bulk protein concentration of 10g/L at two ageing times: 1h and 60h. Straight lines are the best fits using the stratified layer model (see text).

Adsorption time	n_L	*H (nm)*	*Φp (%)*	*Γ (mg/m²)*
1h	1.390±0.007	15±1	32±4	6±1
60h	1.386±0.007	130±8	30±4	53±7

Table 1. Fitting parameters of the ellipsometric angles presented in fig. 8 : Average refractive index n_L and thickness H of the interfacial layer. The associated protein volume fraction Φ_p and surface excess concentration Γ considering a protein layer exclusively in the aqueous phase are given for comparison.

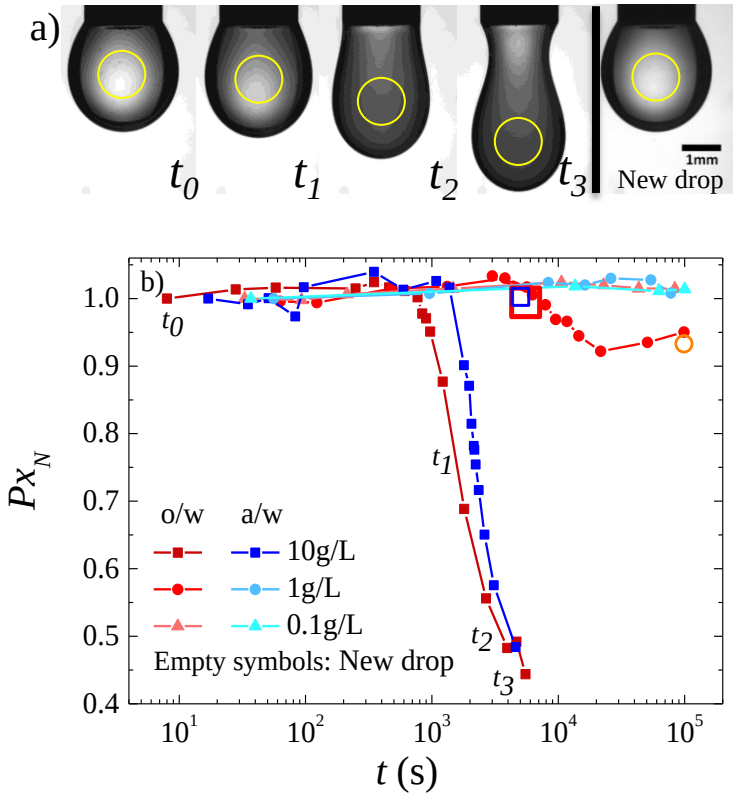

Fig. 9 a) Micrographs of a water in oil drop prepared with a protein solution at 10 g/L at different ageing times: t_0 = 25 s, t_1 = 1440 s, t_2 = 3960 s, t_3 = 5520 s. The last picture shows a new drop formed with the solution aged in the same conditions as the previous drop. The yellow circles display the area in which the grey level is measured. b) Grey level normalized by the drop diameter as a function of the drop ageing time. Red symbols correspond to water in oil drops and blue symbols to water in air drops prepared with solutions of different protein concentrations. The last bigger empty symbols correspond to the grey level for a new drop prepared with the aged solution.

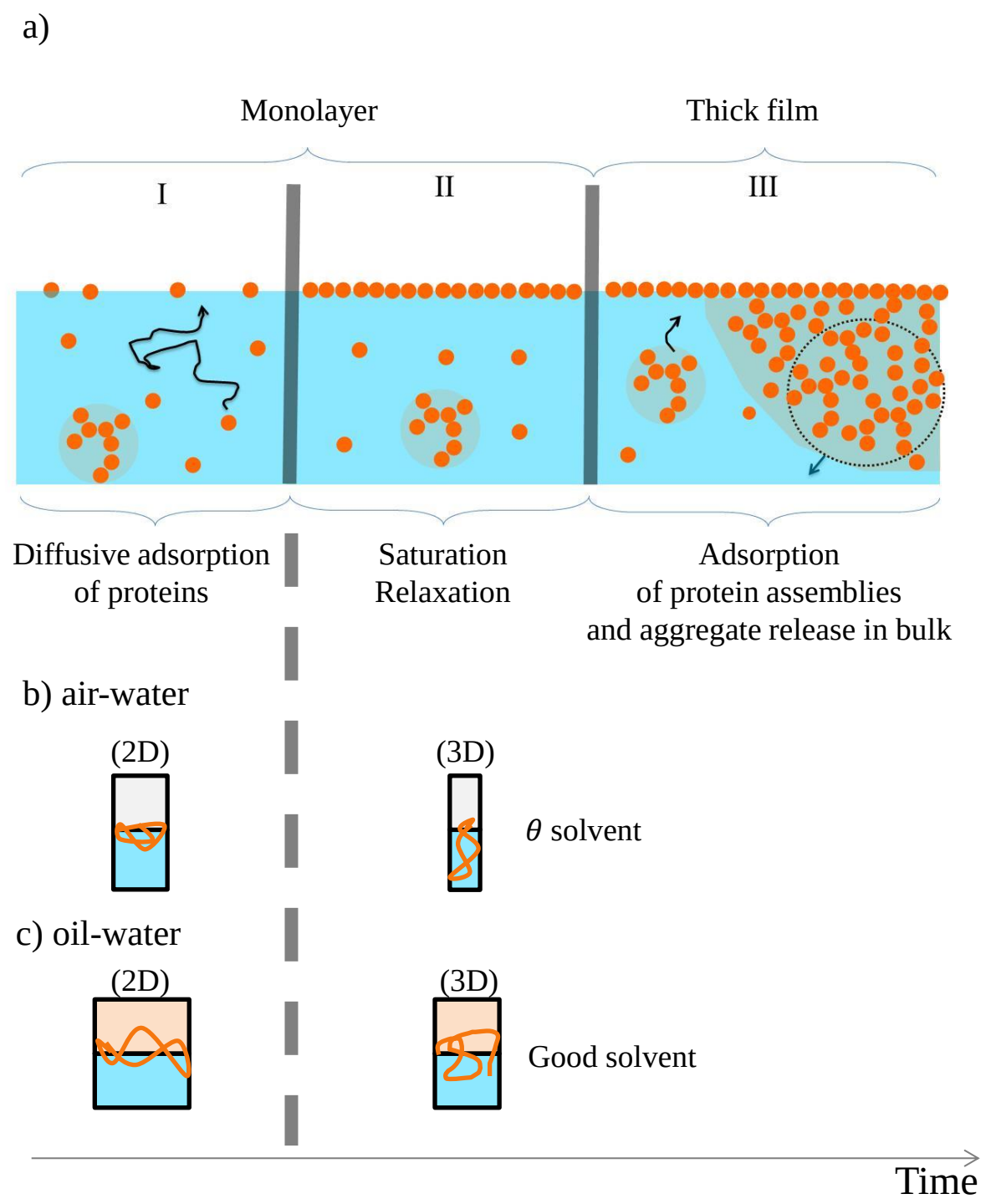

Fig. 10 a) Scheme of the sunflower isolate adsorption at the air-water and oil-water interfaces. The protein compactness and position in the two fluids are detailed for the two interfaces in b) and c). The protein surface area is represented by the width of the box.